CHAPTER 3 DYNAMIC BEHAVIOR OF HIGH DAMPING RUBBER BEARINGS AND LEAD RUBBER BEARING UNDER NEAR-FAULT EARTHQUAKE

3.1 Introduction

The choice of a suitable material model and the determination of its parameters significantly impact the accuracy and reliability of finite element analysis results for rubber components like tires, engine mounts, and rubber bearings. Typically, two types of mechanical models are employed for rubber materials: hyper-elastic and hyper-viscoelastic models. The former is suitable for simpler problems where time effects can be disregarded, while the latter is essential for analyses involving time-dependent factors, such as dissipated energy determination in cyclic loading (hysteresis). Despite extensive research on hyper-elastic models, hyper-viscoelastic models have received less attention, and further work is needed to document and determine their parameters adequately.

The rubber material is derived from Hevea brasiliensis latex, natural rubber, initially known as "Caoutchouc," was termed "rubber" by Joseph Priestley in 1770. Fisher introduced "elastomer" in 1939 for synthetic rubber-like materials. Charles Goodyear's 1839 vulcanization discovery and DuPont's 1931 Neoprene creation revolutionized rubber properties. Fillers, accelerators, anti-ozonants, and antioxidants improve rubber compounds. Natural rubber pads absorbed impact in a Melbourne rail bridge in 1889. Eugene Freyssinet's 1954 patent paved the way for widely used multilayer rubber bearings in earthquake-resistant designs [171]. In 1981, Robinson integrated lead cores into rubber bearings, resulting in the creation of Lead Rubber Bearings (LRB), aimed at improving energy dissipation [172]. The HDRB is exemplified by the 1985 Foothill Communities Law and Justice Center, offer high

stiffness and damping at low shear strains and increased resilience under major earthquakes. Modeling HDRB behavior in seismic design considers factors like creep, rate dependence, mechanical properties, manufacturing variations, and environmental influences [173].

This chapter employs Abaqus CAE 2020 software to validate the static analysis of the LRB model with existing experimental and numerical analysis. Subsequently, the LRB and HDRB are analyzed for dynamic response, comparing acceleration responses at the base and top of the loading plate under ground motion inputs. For dynamic analysis, five near-fault earthquakes are selected from PEER NGA West2 records. Despite extensive research on various isolation systems, including LRB and HDRB, there is a notable scarcity of studies examining the dynamic performance in relation to their mechanical characteristics and material properties. The chapter investigates the impact of seismic isolators, specifically HDRB and LRB, on key seismic parameters. The uniqueness of the work lies in its comparative analysis of these base isolators under various seismic events, providing valuable insights for isolator design. A micro- modeling of the isolator is performed using finite element modeling software ABAQUS, and both LRB and HDRB are subjected to different near-fault ground motions to gain insights into their dynamic response. The results are compared with the input earthquake values, and the response reduction is presented as a percentage decrease in acceleration response. Additionally, the time-displacement response is provided for the Imperial Valley and Managua earthquake records.

3.2 Material Properties, Dimensions and Loading Condition

When selecting numerical models for LRB and HDRB in Abaqus, prioritize accuracy, reliability, and compatibility. The materials for models must be chosen that accurately represent hyperelastic rubber and lead behavior under dynamic loading, ensuring they can

perform dynamic analysis and simulate contact with surrounding structures accurately. The models must be validated against experimental data, consider computational efficiency for numerical simulation in Abaqus.

The LRB used in this study is the Skellerup150 isolator, which is listed in the Skellerup Industries manufacturer's catalogue [174]. The inclusion of steel in rubber isolators is crucial for mitigating excessive strains under vertical loads and is commonly represented as an elastoplastic material. Steel's properties include a yield stress of 240 MPa, a Poisson's ratio of 0.3, and an elastic modulus of 210 GPa. Lead, with a crystal structure undergoing alterations with increasing displacement, is characterized by a yield stress of 19.5 MPa, a Poisson's ratio of 0.43, and a modulus of elasticity of 18000 MPa. The assembly comprises two top and bottom loading steel plates, each with a diameter of 601 mm and a thickness of 31.8 mm. Additionally, there are two fixing steel plates (top and bottom) with a diameter of 431 mm and a thickness of 25.4 mm. The configuration includes 11 rubber layers, each with a diameter of 431 mm and a thickness of 9 .5 mm, as well as 10 steel shims measuring 431 mm in diameter and 3.0 mm in thickness. At the core is a central lead core with a diameter of 116.8 mm and a height of 185 mm. According to the specifications, the design compressive load is 667 kN, and the lateral design displacement is 0.1524 m [74].

Before moving to dynamic analysis, a preliminary static analysis is performed to optimize the dimensions of the bearing. The analysis of the LRB is conducted using ABAQUS CAE (User's Manual V6.14). Initially, the model is subjected to vertical static loadings. After applying a vertical compressive load of 667 kN, a cyclic horizontal displacement with an amplitude of ±152.4 mm is applied, based on the specified dimensions. The analysis includes analytical results from numerical simulations conducted in Abaqus. A comparison is made with the force-displacement curves provided by the manufacturer and Doudoumins 2005, illustrated in Figure 3.1.

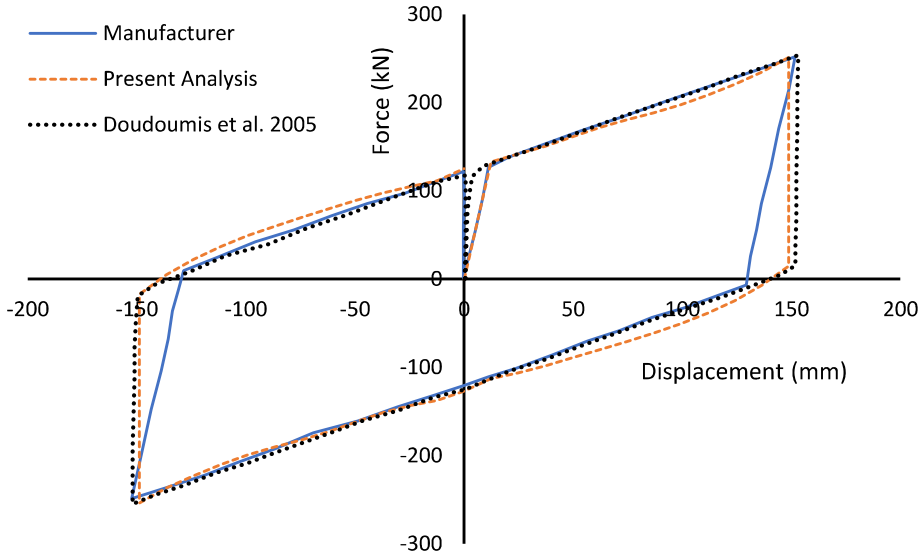

Figure 3.1 Comparison of the force-displacement curves obtained from analytical (Abaqus), experimental and Doudoumis (2005) results.

3.2.1 Selecting a Rubber Constitutive Model for Dynamic Analysis

Rubber is identified as an incompressible material, retaining a constant volume during deformations, which classifies it as isochoric. In rubber compounds, volume alterations are minimal, nearing incompressibility. This results in a Poisson's ratio of 0.5, constraining the use of classical computational mechanics for stress and strain calculations. The elastic

characteristics of rubber in terms of potential strain energy function U in terms of Green's deviatoric strain invariants are as follows:

$$U = f(I_1, I_2, I_3) \tag{3.1}$$

I_1, I_2, I_3 are first, second and third deviatoric strain invariant of the green deformation tensor in terms of $\lambda_1, \lambda_2, \lambda_3$.

$$I_1 = \lambda_1^2 + \lambda_2^2 + \lambda_3^2 \tag{3.2}$$

$$I_2 = \lambda_1^2\lambda_2^2 + \lambda_2^2\lambda_3^2 + \lambda_3^2\lambda_1^2 \tag{3.3}$$

$$I_3 = \lambda_1^2\lambda_2^2\lambda_3^2 \tag{3.4}$$

The rubber's hyper-elasticity is characterized by the Yeoh model, and its damping response is modeled using the Prony series viscosity model. A comprehensive overview of both the Yeoh hyper-elasticity model and the Prony series viscosity model is available in the accompanying Table 3.1 and Table 3.2.

3.2.1.1 Yeoh Model

The strain energy function for the Yeoh model

$$U = C_{10}(\bar{I}_1 - 3) + C_{20}(\bar{I}_1 - 3)^2 + C_{30}(\bar{I}_1 - 3)^3 + \frac{1}{D_1}(J^{el} - 1)^2 + \frac{1}{D_2}(J^{el} - 1)^4 + \frac{1}{D_3}(J^{el} - 1)^6 \tag{3.5}$$

For N=3, the equation can be written as:

$$U = \sum_{i=1}^{3} C_{10}(\bar{I}_1 - 3)^i + \sum_{i=1}^{3} \frac{1}{D_i}(J^{el} - 1)^{2i} \tag{3.6}$$

C_{i0}, D_i are material constants, N= material constant (positive numbers N=1,2,3), μ, λ_m and D, are temperature-dependent parameters D = $\frac{2}{K}$; and $\bar{I}_1 = \bar{\lambda}_1^2 + \bar{\lambda}_2^2 + \bar{\lambda}_3^2$ and $\bar{I}_2 = \bar{\lambda}_1^{(-2)} +$

$\bar{\lambda}_2^{(-2)} + \bar{\lambda}_3^{(-2)}$, where $\bar{\lambda}_i = J^{-\frac{1}{3}}\lambda_i$; J= Jacobean determinant where $J = \lambda_1\lambda_2\lambda_3$, J^{el} is the elastic volume ratio, and K is the bulk modulus. The μ_i and α_i are constants which depend upon shear behaviour and D_i is compressibility. Figure 3.2 displays the rubber specimen's strain-stress curve (black line), with Figure(a) demonstrating alignment between test data and the Yeoh model. In Figure (b), the relaxation data is compared with the Prony model [175].

Table 3.1 Parameters for the Yeoh hyper-elasticity model applied to rubber material [175]

C_{10}	C_{20}	C_{30}
0.206	0.013	-0.000059

Table 3.2 Coefficients for the Prony series in rubber specimens [175]

$\boldsymbol{i}$	$\boldsymbol{G_i}$	$\boldsymbol{t_i}$
1	0.25	0.103
2	0.11	2.664
3	0.08	26.06
4	0.25	924.24

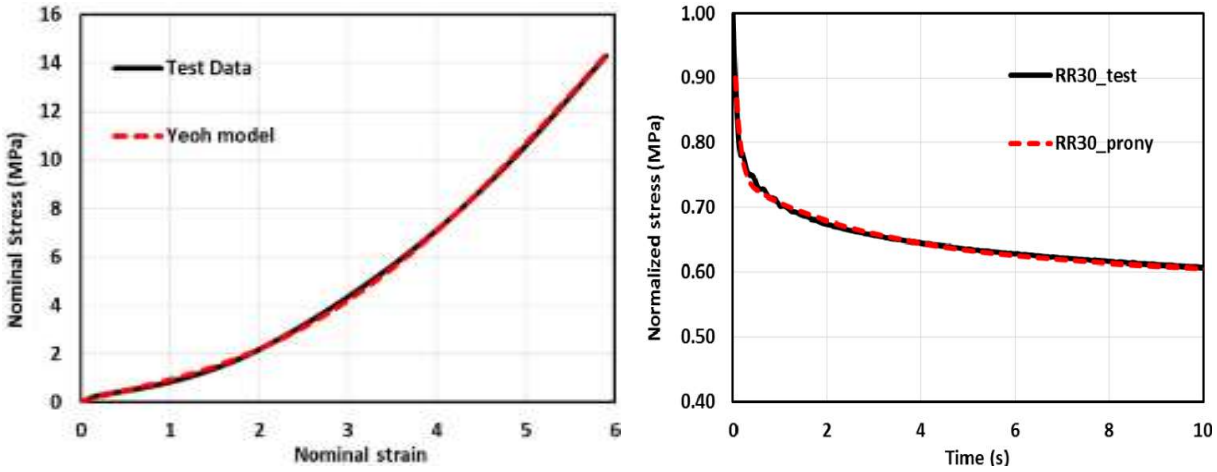

(a) (b)

Figure 3.2 The uniaxial tensile test (a) results (black line) for the rubber specimen, along with the relaxation test results (b), are compared with their respective numerical models, represented by the red line. [175]

3.3 Mechanical parameters of LRB and HDRB

Total thickness of rubber

$$T_r = nt_r \tag{3.7}$$

where n is number of rubber layers, t_r is the thickness of the single rubber layer and T_r is total rubber layer thickness

Total height of the elastomeric rubber bearing

$$h = nt_r + (n-1)t_s \tag{3.8}$$

where n is number of rubber layers, t_r is the thickness of the single rubber layer, t_s thickness of single layer steel shim and T_r is total rubber layer thickness

Bonded rubber area

$$A = \frac{\pi}{4}[(D_0 + t_c)^2 - D_i^2] \tag{3.9}$$

Where, t_c is the rubber cover thickness, D_0 is the outer diameter and D_i is the inner thickness

or lead core diameter (for LRB and for HDRB $D_i = 0$)

The zero-displacement force intercept (Q_d) in a LRB is determined by the shear yield strength of the lead (σ_L) and the area of cross-section for the lead plug (A_L). The characteristics strength for the bearing

$$Q_d = \sigma_L A_L \tag{3.10}$$

The second-slope stiffness (K_d) refers to the elastomeric component stiffness of the bearing. At a specific horizontal displacement (d), the effective or secant stiffness of the LRB is given by:

$$K_{\text{eff}} = \frac{Q_d}{d} + K_d \tag{3.11}$$

Shape factor, is defined individually for a rubber layer as:

$$S = \frac{D_o - D_i}{4t_r} \tag{3.12}$$

The steel shims confine the rubber at the bond interface. The shim spacing (or thickness of rubber layer) regulates the bulging around the perimeter, influencing the compression modulus (E_c) of the elastomeric layer.

$$E_c = \left(\frac{1}{6GS^2F} + \frac{4}{3K_{bulk}}\right)^{-1} \tag{3.13}$$

Where, G is shear modulus, K_{bulk} is bulk modulus of rubber, S is shape factor, central hole factor $F = \frac{(r_d)^2+1}{(r_d-1)^2} + \frac{1+r_d}{(1-r_d)ln(r_d)}$, $r_d = \frac{D_o}{D_i}$

The tight arrangement of steel plates, or thin rubber layers, generates a substantial shape factor, leading to increased vertical stiffness.

$$K_v = \frac{AE_c}{T_r} \tag{3.14}$$

The overall rubber thickness (T_r) serves to offer the essential low horizontal stiffness required to extend the fundamental period of the system. Simultaneously, the tight arrangement of

intermediate steel plates contributes substantial vertical stiffness and shear modulus is given as G and bonded rubber area (A). It's important to note that the steel shim plates do not influence the calculated horizontal stiffness of the bearing.

$$K_h = \frac{GA}{T_r} \tag{3.15}$$

Torsional Stiffness

$$K_t = \frac{2GI_s}{h} \tag{3.16}$$

Effective Period

$$T_{\text{eff}} = 2\pi\sqrt{\frac{W}{K_{\text{eff}}.g}} \tag{3.17}$$

Where, W is the seismic weight of the structure supported by the isolation unit g is gravitational acceleration

Effective stiffness

$$K_{\text{eff}} = \frac{W}{g}\left(\frac{2\pi}{T}\right)^2 \tag{3.18}$$

Hysteresis loop defined the energy dissipation per cycle,

$$W_D = 2\pi K_{\text{eff}}\beta D^2 \tag{3.19}$$

The energy dissipated per loading cycle (E_{loop}) and the effective stiffness (K_{eff}) is determined based on the peak displacements, Δ^+ and Δ^-.

$$\beta_{\text{eff}} = \frac{2}{\pi}\frac{E_{loop}}{K_{\text{eff}}(|\Delta^+|+|\Delta^-|)^2} \tag{3.20}$$

Damping reduction factor

$$\frac{1}{B} = 0.25(1 - ln\beta_{\text{eff}}) \tag{3.21}$$

The design and construction of the isolation system must ensure resilience to, at the very least, the maximum displacement D ascertained through the upper and lower bound characteristics, particularly in the most critical horizontal response direction.

$$D = \frac{gS_aT_{\text{eff}}^2}{4\pi^2 B} \tag{3.22}$$

The force-deflection properties of an isolation system should be determined through cyclic load tests conducted on prototype isolation unit. For each loading cycle, the effective stiffness of the isolator, denoted as K_{eff}, must be calculated as per the specified

$$K_{\text{eff}} = \frac{|F^+|+|F^-|}{|\Delta^+|+|\Delta^-|} \tag{3.23}$$

Here, F^+ represents the positive force at the maximum positive displacement Δ^+, and F^- denotes the negative force at the minimum negative displacement Δ^- as shown in Figure 3.3.

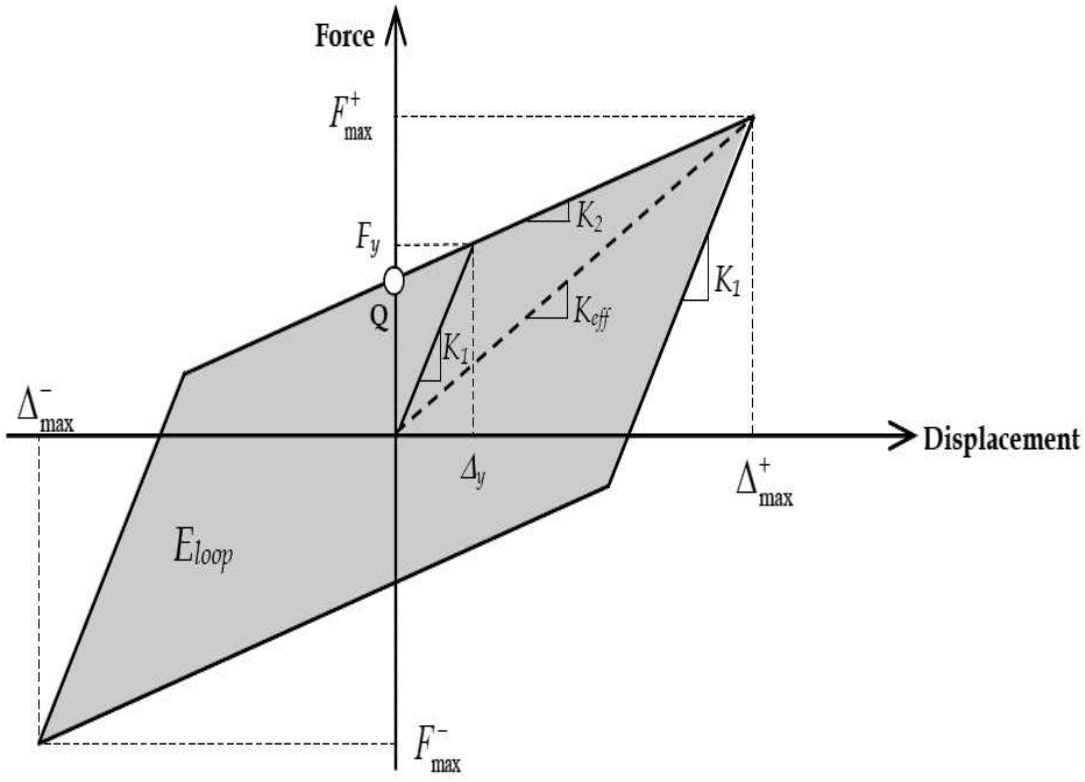

Figure 3.3 Force-Displacement Hysteretic Characteristic of an Isolator (IS 1893 Part 6)

3.3.1 Modelling of HDRB for Dynamic Analysis

The HDRB was modeled in Abaqus CAE 2020 software, with its four parts (Loading Plate, Fixing Plate, Steel Plate, and Rubber Plate as shown in Figure 3.4) created according to properties outlined in the 'Material Properties and Dimensions' section. The model was constructed in the Parts module, with material characteristics such as Poisson's coefficient, modulus of elasticity, density, and plastic properties, including visco-elastic coefficients and Yeoh model coefficients are defined. These properties were assigned to the respective sections, and the parts were assembled together.

To facilitate the dynamic analysis, two reference points are positioned at the centroids of the top and bottom surfaces of the model as shown in Figure 3.5. The degrees of freedom for these surfaces are linked to their corresponding reference points. These reference points serve as anchors for applying boundary conditions and loading scenarios to the bearing. The simulation applied a general method with analysis procedure as Dynamic Implicit in the step module. The Interaction module in ABAQUS serves to define contact behaviors, such as friction or heat, between layers. It also allows for the specification of how degrees of freedom are constrained and how parts are connected. In this study, the Tie constraint is utilized to attach the parts of the isolators, ensuring their cohesive movement as a single unit. The bearing was meshed to create 9222 elements. For the steel material, the C3D8R *Hex* element type (an 8-node linear brick with reduced integration and hourglass control) was selected, while for the visco-hyperelastic rubber material, the C3D20H *Hex* element type (a 20-node quadratic brick with hybrid linear pressure) was chosen. A concentrated force of 667kN was applied at the top of the loading plate of the bearing, and ground motion was applied at its bottom surface.

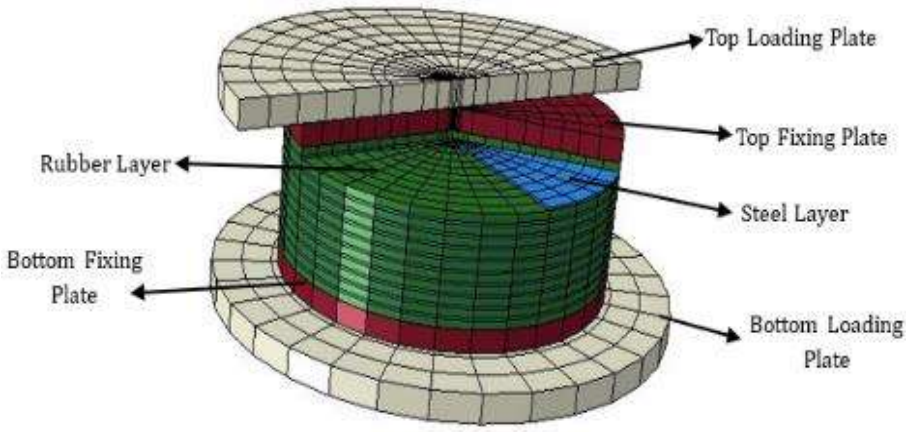

Figure 3.4 Schematic representation of the HDRB with its components

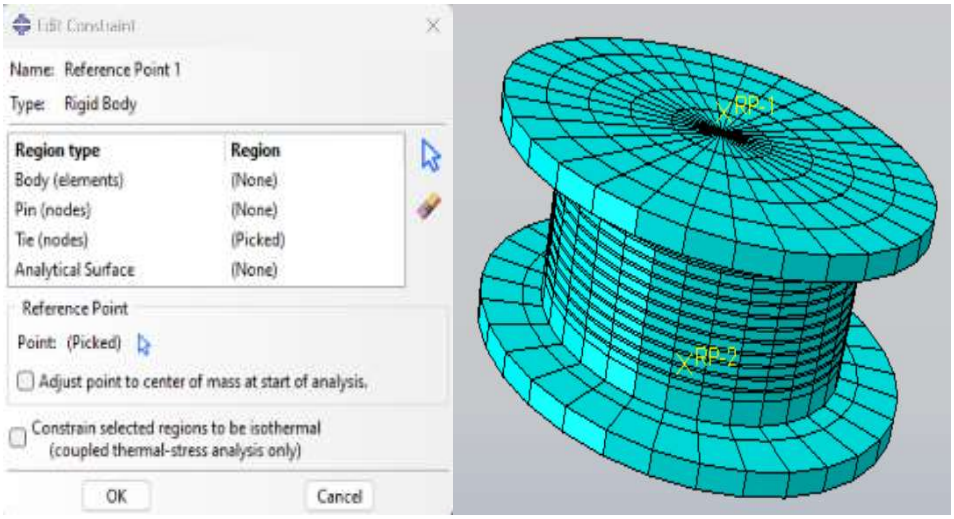

Figure 3.5 Diagram depicts the reference point RP1 and RP2 at the top and bottom of the bearing

3.3.2 Modelling of Lead Rubber Bearing for Dynamic Analysis

The Lead Rubber Bearing was modeled in Abaqus CAE 2020 software, with its five parts (Loading Plate, Fixing Plate, Lead Core, Steel Plate, and Rubber Plate as shown in Figure 3.6) created based on properties outlined in the 'Material Properties and Dimensions' section. The simulation used a general method with analysis procedure is used as Dynamic Explicit in the step module, employing Tie constraints to connect the parts. The bearing was meshed with

4424 *Hex* elements, using the C3D8R element type (an 8-node linear brick with reduced integration and hourglass control). A concentrated force of 667kN was applied at the top of the loading plate of the bearing as shown in Figure 3.7, and ground motion was applied at its bottom surface.

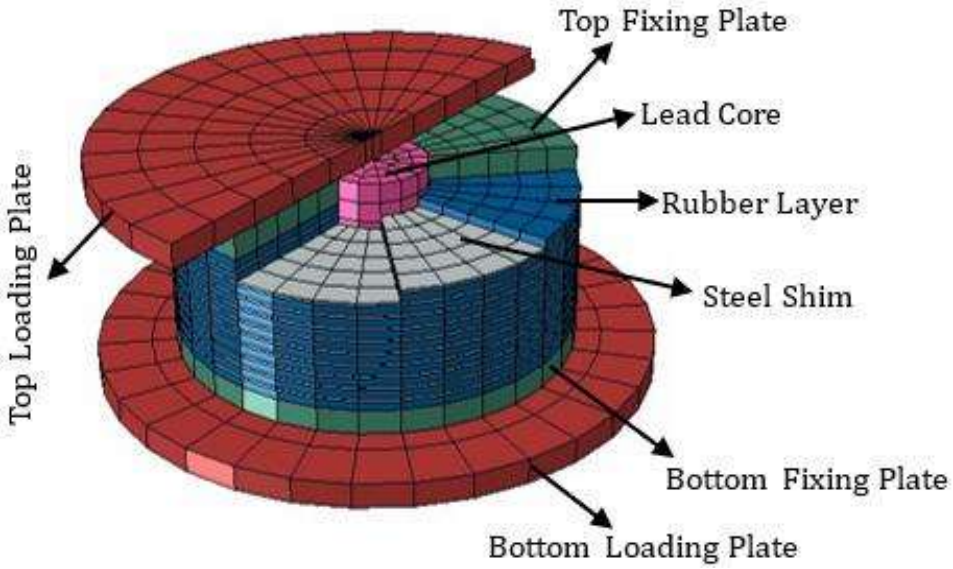

Figure 3.6 Schematic representation of Lead Rubber Bearing

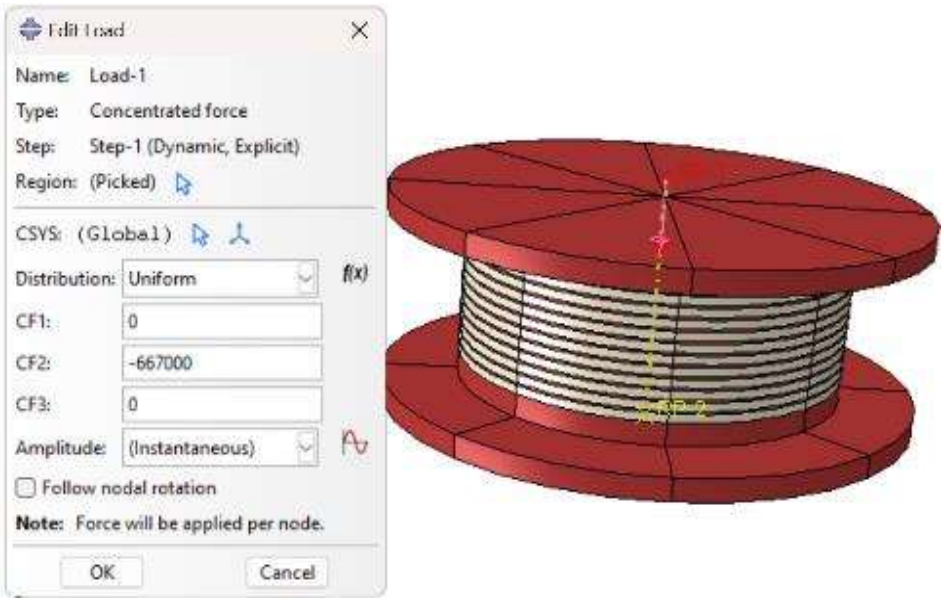

Figure 3.7 Diagram depicts the applied concentrated load on LRB

3.4 Properties of the Near-Fault Ground Motions

To examine the seismic performance of rubber bearings under earthquake excitations, five intense near-field ground motion records were chosen from the Pacific Earthquake Engineering Research Center [176], as listed in the Table 3.3. Near-fault ground motions are discerned by their long-period pulses and substantial ground displacements, which are notably greater than those observed in far-fault ground motions. Using the following earthquake specifications: Magnitude 7 > M_w > 6.0 and Distance (R) < 10 km, a search was conducted in the PEER NGA West2 Ground Motion Database.

Table 3.3 Properties of the applied near-fault ground motions Records

S.No.	Earthquake Record	Station Name	Year	Mechanism	RSN	Magnitude (M_w)	R_{jb} (km)	R_{rup} (km)	V_s30 (m/s)	PGA (g)	PGV (cm/s)	PGD (cm)
1.	Imperial Valley	El Centro Array #9	1940	Strike slip	6	6.95	6.09	6.09	213.4	0.233	31.29	18.44
2.	Managua, Nicaragua	Managua, ESSO	1972	Strike slip	95	6.24	3.51	4.06	288.7	0.354	28.41	6.096
3.	Loma Prieta	Saratoga,	1989	Reverse Oblique	802	6.93	7.58	8.5	380.8	0.369	47.32	26.53
4.	Northridge	Arleta Nordhoff	1994	Reverse	949	6.69	3.3	8.66	297.7	0.329	29.28	9.49
5.	The Kocaeli	Yarmica	1999	Strike Slip	1176	7.51	1.38	4.83	297	0.285	70.86	63.12

3.5 Comparison of the acceleration response

The study examined the key features of the bearings and compared the input earthquakes reduced at the top of both LRB and HDRB. The inclusion of a lead core in the rubber bearing significantly decreased earthquake responses. The comparative results of Imperial Valley, Managua, Kocaeli, Northridge and Loma Prieta are shown in Figure 3.8, Figure 3.9, Figure 3.10, Figure 3.11 and Figure 3.12, respectively. The bearings exhibited effective behavior

during the input time history earthquakes, with maximum response reductions of 68.42% for the Kocaeli earthquake in the case of LRB and 61.80% for the Northridge earthquake in the case of HDRB.

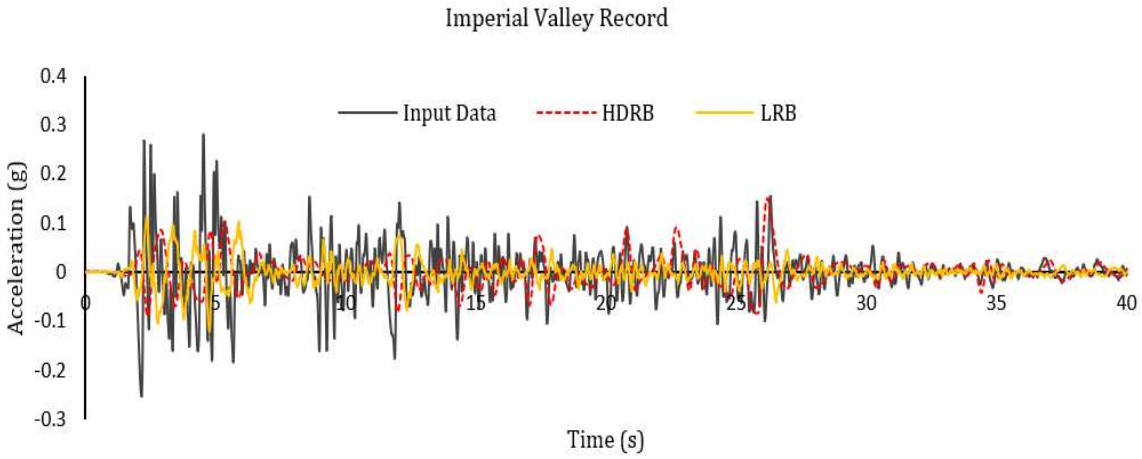

Figure 3.8 Comparison of the Top bearing acceleration obtained from the dynamic analysis of the HDRB and LRB models under the input Imperial Valley earthquake.

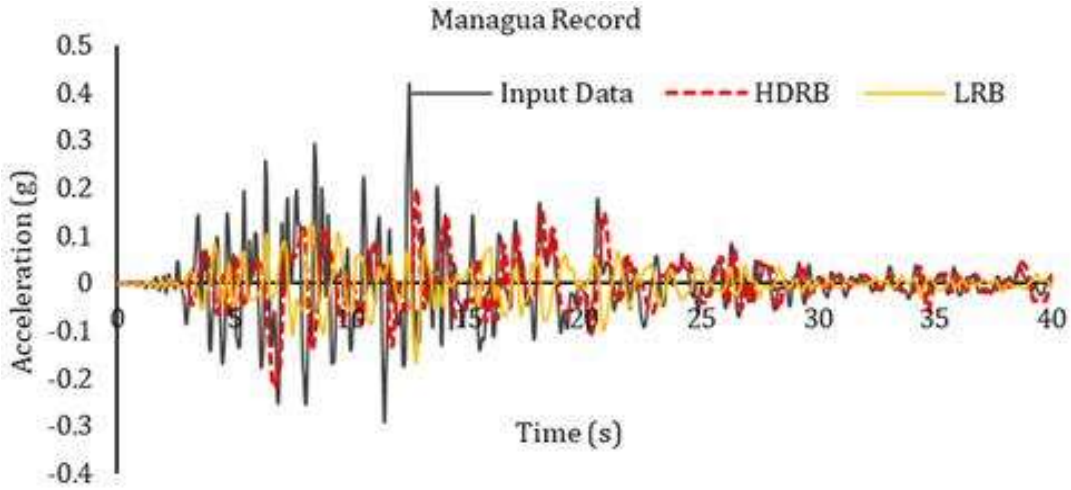

Figure 3.9 Comparison of the Top bearing acceleration obtained from the dynamic analysis of the HDRB and LRB models under the input Managua earthquake.

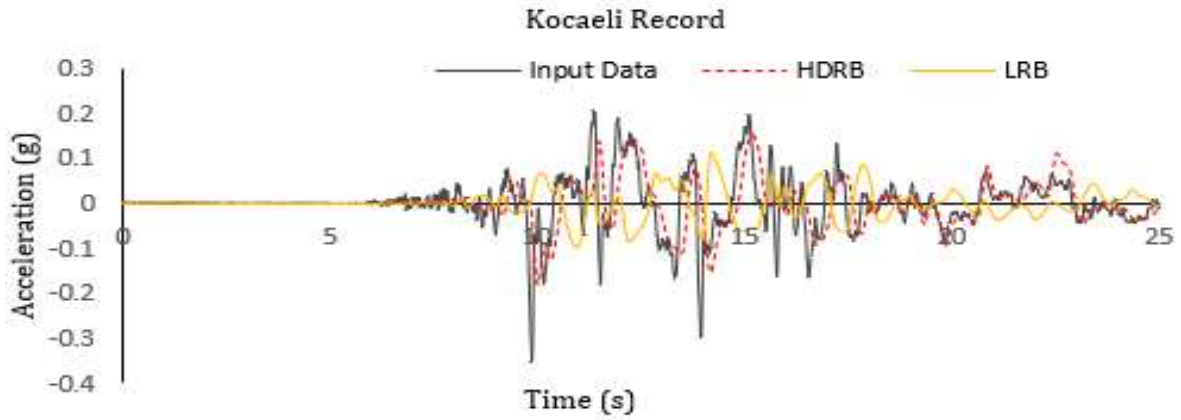

Figure 3.10 Comparison of the Top bearing acceleration obtained from the dynamic analysis of the HDRB and LRB models under the input The Kocaeli earthquake.

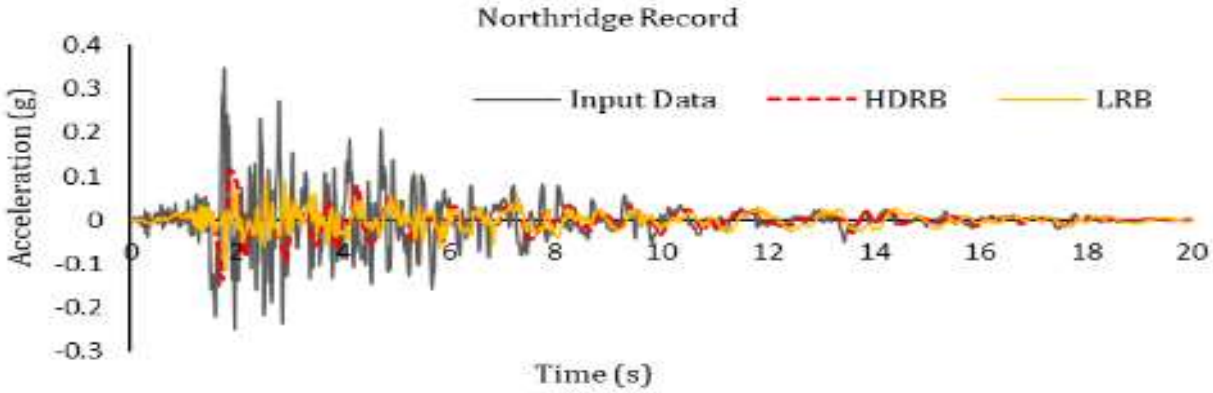

Figure 3.11 Comparison of the Top bearing acceleration obtained from the dynamic analysis of the HDRB and LRB models under the input Northridge earthquake.

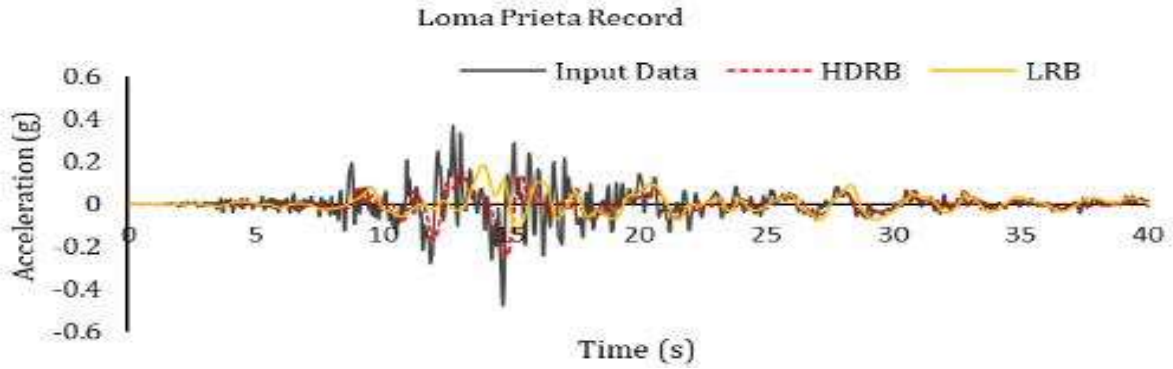

Figure 3.12 Comparison of the Top bearing acceleration obtained from the dynamic analysis of the HDRB and LRB models under the input Loma Prieta earthquake.

3.6 Result and Discussion

The LRB undergoes a general static analysis procedure under a vertically concentrated load and subjected to cyclic lateral load, with the bottom end of the bearing fixed. A force-displacement curve is generated, and the results are compared with experimental and literature data. It was noted that the analyzed model closely aligns with both the manufacturer's specifications and previously analyzed results. Following optimization of the model for static analysis, the bearing is subsequently analyzed for dynamic behavior. The studies were performed [177][178][179][103] to evaluate the dynamic efficiency of the LRB and HDRB. The study conducted by Belbachir [180] shows a 54% reduction in acceleration for the HDRB+FVD isolated system compared to the fixed-base structure. The nonlinear dynamic analysis conducted on a fixed-base RC structure and three different base-isolated RC structures (employing HDRB, LRB, and elastomeric spring damper systems) provided the basis for a comparative analysis. This analysis includes the time history of base acceleration, base shear, base displacements, inter-story drifts over time, and peak base shear values for each system [178]. Further, the study was performed to assessed dynamic responses of isolated structures, including crack distribution, acceleration, displacement, internal forces of bearings, and beam strains near failure. Sudden bearing failure, coupled with horizontal earthquakes, led to significant vertical deformation and impact. This affected adjacent and non-adjacent bearings, increasing the risk of overturning collapse. Vertical and low-frequency earthquake components notably influenced dynamic responses and damages, especially at bearing failure points [179]. In this study, the isolated bearing was simulated using ABAQUS CAE 2020 and subjected to time history records from the Imperial Valley, Managua, Loma Prieta, Northridge, and The Kocaeli events.

3.6.1 Validation of LRB and Analysis of HDRB

The response of the Lead Rubber Bearing (LRB) has been validated against experimental results from the manufacturer and numerical simulation analysis by Doudoumis using ADINA, as illustrated in Figure 3.1. Additionally, a numerical simulation of the HDRB was conducted to analyze its force-displacement response as shown in Figure 3.13. As the bearing undergoes cyclic loading, it exhibits a characteristic behavior in which the applied force increases progressively with displacement. This is accompanied by a gradual stiffening of the bearing structure. Consequently, the displacement of the bearing is met with resistance, resulting in a nonlinear response where the force needed to induce further displacement increases gradually. This behavior is a result of the high damping features of the rubber material within the bearing, which effectively dissipates energy and attenuates vibrations, contributing to the overall stability and performance of the bearing system. The analysis of HDRB and LRB revealed that the lead core in the LRB substantially enhances its performance. The static analysis showed good agreement between the analytical results and the experimental data, validating the precision of the models. These findings confirm the suitability of the numerical models for further dynamic analyses. Moreover, it highlights the efficacy of both LRB and HDRB in fortifying structures against seismic forces, emphasizing their role in bolstering structural resilience.

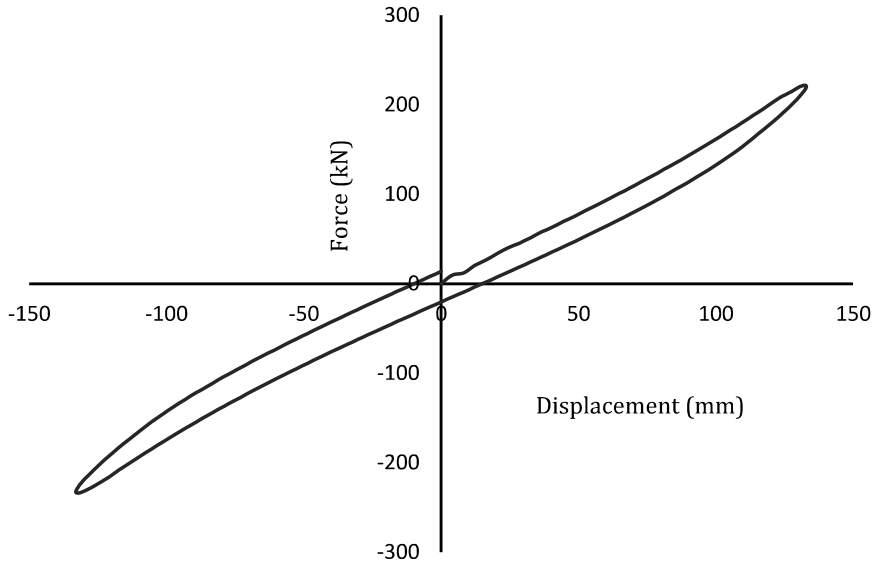

Figure 3.13 Force-Displacement curve of the HDRB subject to horizontal cyclic loading

3.6.2 Acceleration Response

The results, based on accelerations at the top loading plate of the bearing, indicate that the isolation system was effectively activated during seismic events, ensuring the decoupling of motion between the superstructure and the foundations. Numerical analysis shows that the lead rubber bearing achieved a higher reduction in response compared to the HDRB. Specifically, the reduced acceleration responses in percentage are shown in Table 3.4 and the acceleration response in terms of 'g' for input, HDRB and LRB are shown in Figure 3.14. A notable decrease in the acceleration response at the top of the bearing was observed. This phenomenon indicates the effective dissipation of energy within the bearings, leading to reduced transmission of forces and vibrations to the superstructure. Such behavior is a key characteristic of these bearings, highlighting their ability to absorb and dissipate seismic energy, thereby safeguarding the structure against excessive vibrations.

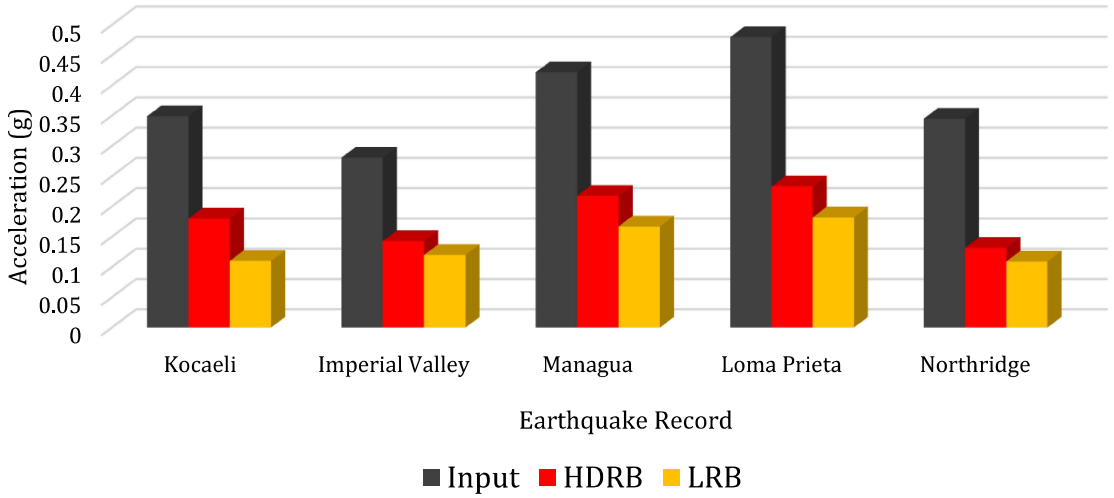

Figure 3.14 Maximum acceleration at the top of the bearing with different input of the Time History earthquakes

Table 3.4 Shows the acceleration response reduction for HDRB and LRB for input earthquake records

S.No.	Earthquake Records	HDRB response	LRB response
1.	The Kocaeli	48.42%	68.42%
2.	Imperial Valley	49.12%	57.24%
3.	Managua	48.35%	60.39%
4.	Loma Prieta	51.42%	62.05%
5.	Northridge	61.80%	68.41%

3.6.3 Displacement Response

The displacement response at the top of the bearing is crucial for understanding structural behavior under seismic loading. It reveals how effectively bearings accommodate deformations and isolate the superstructure. A minimal or decreasing displacement indicates efficient energy dissipation and structural flexibility, reducing transmitted seismic forces. This highlights LRB and HDRB ability to enhance seismic capacity by mitigating ground motion

impact and preventing excessive deformations. To prevent the overturning of isolators, it is crucial to restrict the horizontal displacement of the isolator. As per Chinese Code for the Seismic Design of Buildings, the maximum horizontal displacement of a rubber bearing during a ground motion should not exceed 0.55 times its effective diameter [120]. The displacement responses of the LRB for the Imperial Valley earthquake and the HDRB for the Managua earthquake, as illustrated in the respective Figure 3.15 and Figure 3.16, are provided. However, these responses, being at the top of the bearing, may not entirely reflect the actual behavior as it would occur within a complete building-bearings system.

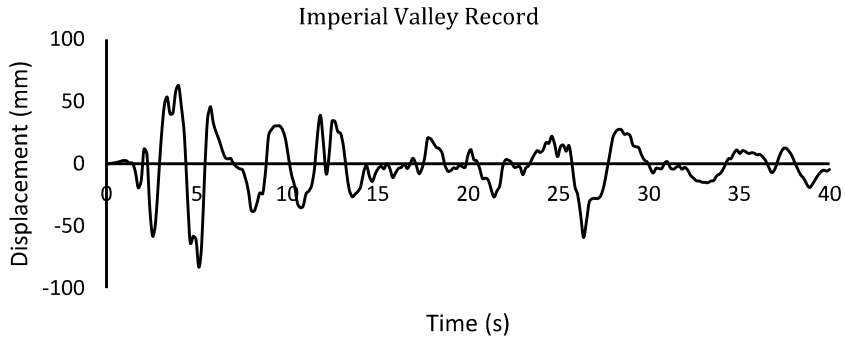

Figure 3.15 The Displacement response of the lead rubber bearing for time history function Imperial Valley

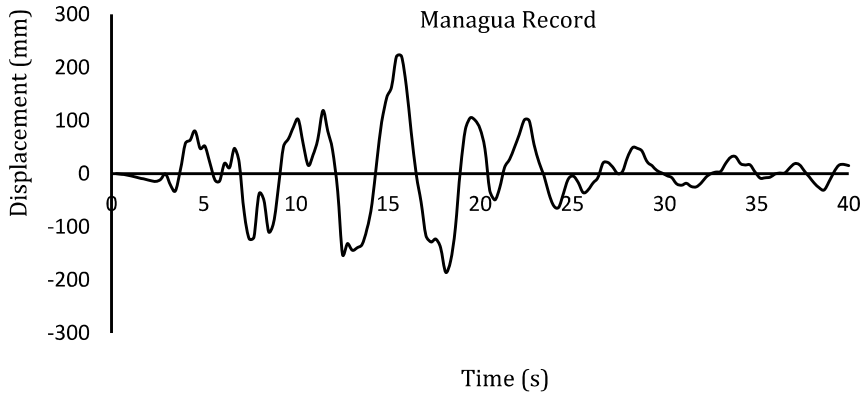

Figure 3.16 The Displacement response of the high damping rubber bearing for time history function Managua

3.7 Summary

In summary, the study comprehensively validated two types of isolators, LRB and HDRB, through a meticulous process involving static and dynamic analyses using 3D Finite Element (FE) models in Abaqus. The dynamic analysis revealed promising results, particularly in terms of acceleration and displacement responses. The bearings exhibited efficient energy dissipation, leading to reduced transmitted forces and vibrations to the superstructure. Furthermore, they demonstrated the capacity to withstand significant deformations, effectively protecting the superstructure from ground motion. These findings, presented in terms of the acceleration reduction within the bearing, highlight the effectiveness of LRB and HDRB in enhancing the seismic resilience of structures. This suggests their potential to mitigate ground motion impacts and prevent excessive structural deformations.

Finite element micromodels provide detailed insights into the stress, strain, and strength characteristics of LRB and HDRB, aiding in the understanding of their mechanical behavior and facilitating improvements in their design. The inclusion of a lead core in LRB alters stress and strain distribution, highlighting the necessity of micromodels for their study. It is essential to validate basic assumptions regarding material properties and fabrication details to ensure the accuracy of the analysis.

Dynamic analysis of HDRB and LRB in Abaqus is limited by the accuracy of material models for dynamic loading, large deformations, and high loading rates. Contact modeling, crucial for HDRB and LRB, can be challenging to accurately represent in Abaqus, impacting overall performance assessment. Additionally, results may be affected by material and interaction properties of the models, with dynamic analyses being computationally time consuming for complex models.

This research addresses the gap in the literature by focusing specifically on LRB and HDRB, applying ABAQUS software package for numerical simulations and finite element micro-analysis. The results include a comparative analysis of the reduction in input earthquake forces, laying the foundation for future research in this field.